Letter

Thermal difference reflectivity of tilted two-dimensional Dirac materials

M. A. Mojarro [1] R. Carrillo-Bastos [2] and Jesús A. Maytorena [3,*]

[1]*Department of Physics and Astronomy and Nanoscale and Quantum Phenomena Institute, Ohio University, Athens, Ohio 45701, USA*
[2]*Facultad de Ciencias, Universidad Autónoma de Baja California, Apartado Postal 1880, 22800 Ensenada, Baja California, México*
[3]*Centro de Nanociencias y Nanotecnología, Universidad Nacional Autónoma de México,*
Apartado Postal 2681, 22800 Ensenada, Baja California, México

Deviation from perfect conical dispersion in Dirac materials, such as the presence of mass or tilting, enhances the control and directionality of electronic transport. To identify these signatures, we analyze the thermal derivative spectra of optical reflectivity in doped massive tilted Dirac systems. The density of states and chemical potential are determined as preliminary steps to calculate the optical conductivity tensor at finite temperature using thermal convolution. Changes in reflection caused by temperature variations enable the clear identification of critical frequencies in the optical response. By measuring these spectral features in the thermoderivative spectrum, energy gaps and band structure tilting can be determined. A comparison is presented between the spectra of various low-energy Dirac Hamiltonians. Our findings suggest that thermal difference spectroscopy holds promise as a valuable technique for probing interband transitions of two-dimensional Dirac fermions.

Optical spectroscopies allow the investigation of surfaces and interfaces, offering nondestructive, *in situ*, and real-time probing capabilities, with various techniques available such as spectroscopic ellipsometry, differential reflectance, electroreflectance, reflection anisotropy spectroscopy, magneto-optics, and nonlinear spectroscopies [1,2]. Recent methods resolve single nano-objects and subwavelength structures [3], plasmon dynamics [4], organic and biological interfaces [5], graphenelike materials [6], and metasurfaces [7,8].

In the field of two-dimensional (2D) systems, the in-plane optical anisotropy of low-symmetry 2D materials is emerging as a unique characteristic with potential applications in optics, optoelectronics, and photonics [9–11]. Orthorhombic systems such as black phosphorus (BP) [12,13] and group-IV monochalcogenides, monoclinic systems such as 1T′-WTe$_2$ [14], and triclinic materials such as ReS$_2$ [15] present an optical anisotropy due to their anisotropic band structure, which can be modified by band engineering methods. This is an essential difference with anisotropic nanostructures made of symmetric 2D materials, where the anisotropy of the dielectric constant is designed by nanofabrication [16].

The in-plane anisotropy of these materials, along with critical frequencies and optical transitions involving the Fermi level, have been probed through a number of differential and modulation spectroscopy techniques, such as differential reflectance and transmittance spectroscopy [17], anisotropic optical absorption and photoluminescence [16], Raman scattering [16,18], time-domain thermoreflectance [19], azimuthal-dependent reflectance difference spectroscopy [15], or reflection difference microscopy combined with electron transport measurements and atomic force microscopy [20].

Two-dimensional materials with tilted Dirac cones in their energy spectrum are an interesting and currently attractive variant of anisotropic systems. The tilting of the bands introduces an additional source of anisotropy which can significantly modify the optical response [21–29] and provides a rich solid-state space-time platform due to the associated non-Minkowski metric [30–33]. The quasi-2D organic conductor α-(BEDT-TTF)$_2$I$_3$ [34–38] is a well-known example of an anisotropic material which presents a pair of tilted Dirac cones when external pressure is applied [39,40], and even massive Dirac fermions below a critical pressure [41]. Another well-studied tilted system is the 8-*Pmmn* borophene, for which band gap opening [42] and tilt tuning [43] have been predicted.

Herein, we theoretically explore the thermal difference spectroscopy [44–46] to identify relevant features in the optical response of massive tilted 2D Dirac systems at finite temperature. To this end, we first calculate the temperature dependence of the chemical potential and then the optical conductivity through a thermal convolution. This extends our previously reported calculations at zero temperature [22,23]. Then, we evaluate the optical reflectivity at two close temperatures to obtain the derivative of its spectrum, which provides a way to compensate for the reduced structure produced by thermal broadening. The change in reflectivity caused by temperature variation probes the anisotropy of the system and highlights critical points in the optical absorption or reflection spectrum. Thermal difference spectroscopy measures the derivative of the optical spectrum, as in temperature modulation spectroscopy, but without involving modulation of the sample's temperature at a given frequency. In particular, we discuss the possibility of estimating

*jesusm@ens.cnyn.unam.mx

parameters such as tilting or gaps through this thermal derivative approach.

From the electromagnetic scattering problem of optical reflection and refraction at a flat interface made of a 2D system, with conductivities $\sigma_{xx}(\omega, T)$ and $\sigma_{yy}(\omega, T)$, separating two homogeneous media with dielectric constants ϵ_1 and ϵ_2, the optical reflectivity is obtained as $R(\omega, T) = |r_p|^2 \cos^2 \phi + |r_s|^2 \sin^2 \phi$ [22], where ϕ is the angle of polarization of the incident field, ω the frequency, and T the temperature. The Fresnel amplitudes are

$$r_p(\omega, T) = \frac{\epsilon_2 k_z^i - \epsilon_1 k_z^t + 4\pi \left(k_z^i k_z^t/k_0\right)[\sigma_{xx}(\omega, T)/c]}{\epsilon_2 k_z^i + \epsilon_1 k_z^t + 4\pi \left(k_z^i k_z^t/k_0\right)[\sigma_{xx}(\omega, T)/c]}, \quad (1)$$

$$r_s(\omega, T) = \frac{k_z^i - k_z^t - 4\pi k_0[\sigma_{yy}(\omega, T)/c]}{k_z^i + k_z^t + 4\pi k_0[\sigma_{yy}(\omega, T)/c]}, \quad (2)$$

for p ($\phi = 0$) and s ($\phi = \pi/2$) polarizations; $k_0 = \omega/c$, and $k_z^i = k_0 \sqrt{\epsilon_1} \cos \theta_i$, $k_z^t = k_0 \sqrt{\epsilon_2 - \epsilon_1 \sin^2 \theta_i}$ are the normal to the surface components of the incident and refracted wave vectors, respectively, where θ_i is the incidence angle. The frequency and temperature dependence of R_p (R_s) is solely determined by σ_{xx} (σ_{yy}).

In the following, we take the thermal derivative of the reflectivity spectra. To this end, we calculate the normalized difference between $R(T)$ taken at two temperatures [44,46],

$$\frac{R_\nu(\omega, T + \Delta T) - R_\nu(\omega, T - \Delta T)}{[R_\nu(\omega, T + \Delta T) + R_\nu(\omega, T - \Delta T)]/2}.$$

Assuming a small enough ΔT, the quantity $\Delta R_\nu/R_\nu = (1/R_\nu)(\partial R_\nu/\partial T)2\Delta T$ measures the change in reflectivity caused by temperature variation. The thermoderivative is obtained from

$$\frac{\partial R_\nu}{\partial T} = \frac{\partial R_\nu}{\partial \sigma'_{ii}} \frac{\partial \sigma'_{ii}}{\partial T} + \frac{\partial R_\nu}{\partial \sigma''_{ii}} \frac{\partial \sigma''_{ii}}{\partial T}, \quad (3)$$

where $i = x$ (y) if $\nu = p$ (s), $\sigma'_{ii} \equiv \text{Re}(\sigma_{ii})$, and $\sigma''_{ii} \equiv \text{Im}(\sigma_{ii})$. We will show results for p polarization only ($R = R_p$), with $\epsilon_2 = 2\epsilon_1 = 2$; the corresponding spectra for $\nu = s$ are qualitatively similar.

The conductivity tensor at finite temperature can be calculated from a convolution integral between the zero-temperature counterpart, $\sigma_{ij}(\omega; 0, \mu')$, and the peaked function, $\partial f(\mu, \mu')/\partial \mu'$, with $f[\mu(T), \mu'] = (\exp\{\beta[\mu(T) - \mu']\} + 1)^{-1}$, which takes the form [47]

$$\sigma_{ij}[\omega; T, \mu(T)] = \frac{\beta}{4} \int_{-\infty}^{\infty} \frac{\sigma_{ij}(\omega; 0, \mu') \, d\mu'}{\cosh^2\{\beta[\mu(T) - \mu']/2\}}, \quad (4)$$

where μ' is the Fermi energy $\varepsilon_F = \mu(T = 0)$ and $\beta = 1/k_B T$. In this work, the zero-temperature response $\sigma_{ij}(\omega; 0, \mu')$ is evaluated within the Kubo formalism for a massive tilted Dirac system modeled by the time-reversal symmetric Hamiltonian [22],

$$H_\xi(\mathbf{k}) = \xi(\hbar v_t k_y \hat{\sigma}_0 + \hbar v_x k_x \hat{\sigma}_x + \xi \hbar v_y k_y \hat{\sigma}_y) + \Delta \hat{\sigma}_z, \quad (5)$$

with energy spectrum $\varepsilon_\lambda^\xi(k_x, k_y) = \xi \hbar v_t k_y + \lambda \sqrt{(\hbar v_x)^2 k_x^2 + (\hbar v_y)^2 k_y^2 + \Delta^2}$, where the Pauli matrices $\hat{\sigma}_i$ act on a pseudospin space, $\mathbf{k} = (k_x, k_y)$ is the electron wave vector in the vicinity of the $K(K')$ point in the valley

$\xi = +(-)$, while $\lambda = \pm$ specifies the helicity of states in the conduction $(+)$ and valence $(-)$ bands; for the mass term, we take $\Delta > 0$. A thorough study of the optical properties of this model (5) was presented in Refs. [22,23]. This Dirac model describes several anisotropic 2D Dirac fermions in systems such as the organic conductor α-(BEDT-TTF)$_2$I$_3$ [39,40], the 8-$Pmmn$ borophene (with $v_x = 0.86 \times 10^6$ m/s, $v_y = 0.69 \times 10^6$ m/s, $v_t = 0.32 \times 10^6$ m/s) [21], monolayer WTe$_2$ with ($v_x = 0.644 \times 10^6$ m/s, $v_y = 0.365 \times 10^6$ m/s, $v_t = 0.464 \times 10^6$ m/s) [48], or 2D ladder polyborane ($v_x = 0.735 \times 10^6$ m/s, $v_y = 0.397 \times 10^6$ m/s, $v_t = 0.191 \times 10^6$ m/s) [28]. It has also been used in studies of the nonlinear optical response such as the nonlinear Hall effect [49–51], the second-order conductivity induced by the quantum metric dipole [52,53], and nonlinear thermal Hall effects [54].

An interesting feature of the model is that the band gap in each valley is indirect, with a minimum (maximum) of the conduction (valence) band ε_+^ξ (ε_-^ξ) at $\mathbf{k}_\xi = -\xi Q \hat{\mathbf{y}}$ ($+\xi Q \hat{\mathbf{y}}$), where $\hbar v_y Q = \gamma \Delta/\sqrt{1 - \gamma^2}$, with $\gamma = v_t/v_y$ ($0 \leqslant \gamma < 1$) being the tilting parameter. As a consequence, a new region appears for the Fermi level, $\tilde{\Delta} \leqslant \varepsilon_F \leqslant \Delta$ (the "indirect zone"), with $\tilde{\Delta} = \Delta\sqrt{1 - \gamma^2}$, which has a striking effect on the spectrum of interband transitions [22]. We note that the optical response to a long-wavelength external field excludes interband transitions with finite momentum, in particular those with a wave vector close to $\pm \xi 2Q \hat{\mathbf{y}}$, in the vicinity of the gap $2\tilde{\Delta}$. However, the indirect gap manifests itself through the appearance of the indirect zone, which is absent for the untilted or ungapped system ($\gamma \Delta = 0$).

The evaluation of integral (4) requires prior knowledge of the chemical potential μ as a function of temperature. Here, we obtain $\mu(T)$ by solving the transcendental equation that arises from expressing the doping electron density n as a proper integral of the density of states (DOS), and equating n to that at zero temperature for a given Fermi energy [55]. This approach was used in Ref. [56], where the function $\mu(T)$ for several doped and gapped Dirac materials (graphene, silicene, germanene, and MoS$_2$) with a linear density of states was derived. In our work, tilting of the bands in Eq. (5) is an additional component in the calculations.

Thus, to proceed, we first calculate the DOS of our system,

$$D(\varepsilon) = g_s \sum_{\xi, \lambda = \pm} \int \frac{d^2 k}{(2\pi)^2} \delta[\varepsilon - \varepsilon_\lambda^\xi(\mathbf{k})], \quad (6)$$

with $g_s = 2$ being the spin degeneracy and $\delta(\varepsilon)$ the Dirac delta function. We find that the corresponding DOS of the system (5) is electron-hole symmetric and therefore has the following structure:

$$D(\varepsilon) = F(\varepsilon)\Theta(|\varepsilon| - \Delta) + G(\varepsilon)\Theta[1 - |\eta(\varepsilon)|], \quad (7)$$

where $\eta(\varepsilon) = [|\varepsilon| - (\Delta + \tilde{\Delta})/2]/[(\Delta - \tilde{\Delta})/2]$. The function G contributes when the energy is within the indirect zone $|\eta(\varepsilon)| < 1$, while the function F when $|\varepsilon| > \Delta$.

For $|\varepsilon| > \Delta$, the contribution $F(\varepsilon)$ reduces to the expression

$$F(\varepsilon) = \frac{g_s g_v}{2\pi} \frac{|\varepsilon|}{(\hbar v_F)^2} \frac{d(\gamma I_F)}{d\gamma}, \quad (8)$$

where $g_v = 2$ is the valley degeneracy and I_F is the dimensionless integral,

$$I_F = \frac{1}{2\pi} \int_0^{2\pi} \frac{d\theta}{g^2(\theta) - h^2(\theta)}.$$

We define the function $h(\theta) = (v_t/v_F)\sin\theta$ to describe the anisotropy resulting from the tilt of the bands, while $g(\theta) = [(v_x/v_F)^2 \cos^2\theta + (v_y/v_F)^2 \sin^2\theta]^{1/2}$ accounts for the anisotropy of the velocity, where $v_x \neq v_y$. Complex integration gives $I_F = (v_F^2/v_x v_y)(1-\gamma^2)^{-1/2}$, which implies

$$F(\varepsilon) = \frac{g_s g_v}{2\pi} \frac{|\varepsilon|}{(\hbar v_x)(\hbar v_y)} \frac{1}{(1-\gamma^2)^{3/2}}. \tag{9}$$

When $\tilde{\Delta} < |\varepsilon| < \Delta$ [$|\eta(\varepsilon)| < 1$], $G(\varepsilon)$ can be written as

$$G(\varepsilon) = \frac{g_s g_v}{2\pi} \frac{1}{(\hbar v_F)^2} \frac{\partial I_G(\varepsilon)}{\partial \varepsilon}, \tag{10}$$

where

$$I_G(\varepsilon) = \frac{\varepsilon}{\pi} \int_{\frac{\pi}{2}-\theta^*}^{\frac{\pi}{2}+\theta^*} d\theta \, \frac{h(\theta)\sqrt{\varepsilon^2 g^2(\theta) - \Delta^2[g^2(\theta) - h^2(\theta)]}}{[g^2(\theta) - h^2(\theta)]^2},$$

with $\tan\theta^* = (v_y/v_x)\sqrt{[\varepsilon^2 - \tilde{\Delta}^2]/[\Delta^2 - \varepsilon^2]}$. The restricted sector of integration reflects the drastic reduction of the momentum space available for vertical transitions when the energy lies within the narrow stripe between $\tilde{\Delta}$ and Δ, arising from the indirect nature of the gap [22] ($\gamma\Delta \neq 0$). We obtain $I_G(\varepsilon) = \text{sign}(\varepsilon)(\varepsilon^2 - \tilde{\Delta}^2)/[2(v_x/v_F)(v_y/v_F)(1-\gamma^2)^{3/2}]$, which leads to the result $G(\varepsilon) = F(\varepsilon)$. Therefore, from (7), we find, for the DOS of a tilted and gapped Dirac system,

$$D(\varepsilon) = \frac{g_s g_v}{2\pi} \frac{|\varepsilon|}{(\hbar v_x)(\hbar v_y)} \frac{\Theta(|\varepsilon| - \tilde{\Delta})}{(1-\gamma^2)^{3/2}}. \tag{11}$$

Given that the DOS is an even function of energy, the doping electron density, obtained from the difference between the densities of electrons and holes [56,57], can be calculated from

$$n(T,\mu) = \sinh(\beta\mu) \int_0^\infty d\varepsilon \, \frac{D(\varepsilon)}{\cosh(\beta\varepsilon) + \cosh(\beta\mu)}. \tag{12}$$

As a result, we find

$$n = \frac{2}{\pi(\hbar v_x)(\hbar v_y)} \frac{1}{(1-\gamma^2)^{3/2}} \frac{1}{\beta^2} \Lambda[T, \mu(T), \tilde{\Delta}], \tag{13}$$

where

$$\Lambda[T, \mu(T), \tilde{\Delta}] = \beta\tilde{\Delta} \ln\left(\frac{1 + e^{\beta(\mu-\tilde{\Delta})}}{1 + e^{-\beta(\mu+\tilde{\Delta})}}\right)$$
$$+ \text{Li}_2(-e^{-\beta(\mu+\tilde{\Delta})}) - \text{Li}_2(-e^{\beta(\mu-\tilde{\Delta})}),$$

where $\text{Li}_2(x)$ is the dilogarithm function [55,58].

For fixed n and T, the function $\mu(T)$ can be obtained from this expression or in terms of the Fermi energy $\varepsilon_F = \mu(0)$,

$$\varepsilon_F^2 - \tilde{\Delta}^2 = 2(k_B T)^2 \Lambda[T, \mu(T), \tilde{\Delta}]. \tag{14}$$

This equation generalizes the results reported in [56] to include the tilting, such that for $v_x = v_y = v_F$, $\gamma = 0$, the results reported for gapped ($\Delta \neq 0$) or ungapped ($\Delta = 0$) graphene can be recovered. For $\Delta = 0$, the results (9) and (13) give

TABLE I. Density of states, $D(\varepsilon)$, and doping electron density n in terms of the Fermi energy $\varepsilon_F = \mu(0)$, for gapped and/or tilted Dirac systems.

System	$D(\varepsilon)$	n
$\Delta = 0, \gamma = 0$	$\dfrac{2|\varepsilon|}{\pi(\hbar v_F)^2}$	$\dfrac{\varepsilon_F^2}{\pi(\hbar v_F)^2}$
$\Delta \neq 0, \gamma = 0$	$\dfrac{2|\varepsilon|\Theta(|\varepsilon|-\Delta)}{\pi(\hbar v_F)^2}$	$\dfrac{\varepsilon_F^2 - \Delta^2}{\pi(\hbar v_F)^2}$
$\Delta = 0, \gamma \neq 0$	$\dfrac{2|\varepsilon|}{\pi(\hbar v_x)(\hbar v_y)(1-\gamma^2)^{3/2}}$	$\dfrac{\varepsilon_F^2}{\pi(\hbar v_x)(\hbar v_y)(1-\gamma^2)^{3/2}}$
$\Delta \neq 0, \gamma \neq 0$	$\dfrac{2|\varepsilon|\Theta(|\varepsilon|-\tilde{\Delta})}{\pi(\hbar v_x)(\hbar v_y)(1-\gamma^2)^{3/2}}$	$\dfrac{\varepsilon_F^2 - \tilde{\Delta}^2}{\pi(\hbar v_x)(\hbar v_y)(1-\gamma^2)^{3/2}}$

the DOS and the doping density of the tilted system. Table I summarizes the expressions $D(\varepsilon)$ and n when $\gamma\Delta = 0$ and $\gamma\Delta \neq 0$.

In Fig. 1(a), we show the DOS for several Dirac materials. The gapless cases exhibit the usual linear behavior with energy (green solid and dashed lines). The difference in slope arises from two factors: (i) the factor $(1-\gamma^2)^{-3/2}$ due to the tilting, and (ii) the anisotropy of the velocity. This can be interpreted geometrically by noting that $D(\varepsilon) \propto d\mathcal{A}/d\varepsilon$, where $\mathcal{A} = \pi ab$ is the area of the ellipse with semiaxis $a = \sqrt{\varepsilon^2 - \tilde{\Delta}^2}/[(\hbar v_x)\sqrt{1-\gamma^2}]$ and $b = \sqrt{\varepsilon^2 - \tilde{\Delta}^2}/[(\hbar v_y)(1-\gamma^2)]$, which is generated by the cut $\varepsilon_\lambda^\xi(\mathbf{k}) = \varepsilon$ of any of the tilted bands. The anisotropy introduces a further rise in the DOS as the velocity v_F of isotropic bands is replaced by the geometric mean, $\sqrt{v_x v_y}$. Finally, the DOS displays a step in the massive cases (purple and green dashed lines).

In Fig. 1(b), we present the corresponding chemical potentials $\mu(T)$ calculated from Eq. (14) at a fixed positive value of ε_F. The function $\mu(T)$ remains positive in all cases. In the absence of tilting, the presence of a gap leads to a more rapid decrease of $\mu(T)$ as a function of temperature compared to the simplest case of graphene, due to the vanishing density of states in the region, $|\varepsilon| < \Delta$. However, in the case of massive tilting ($\gamma\Delta \neq 0$), the rate of decrease of $\mu(T)$ decelerates compared to gapped graphene, as the window of the vanishing density of states is reduced to $|\varepsilon| < \tilde{\Delta}$. This behavior should be contrasted with certain direct-band-gap transition-metal dichalcogenides with broken electron-hole symmetry, such as MoS_2, where the chemical potential for electron doping switches from positive to negative at sufficiently high temper-
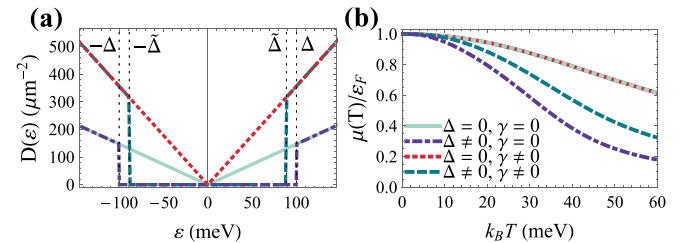

FIG. 1. (a) Density of states and (b) chemical potential $\mu(T)$ of several Dirac materials: graphene ($v_x = v_y$, $\gamma = \Delta = 0$), gapped graphene ($v_x = v_y$, $\gamma = 0$, $\Delta \neq 0$), tilted (8-*Pmmn* borophene, $v_x \neq v_y$, $\gamma \neq 0$, $\Delta = 0$), and massive tilted ($v_x \neq v_y$, $\gamma \neq 0$, $\Delta \neq 0$), with $\varepsilon_F = 110$ meV. For the gapped cases, we take $\Delta = 100$ meV.
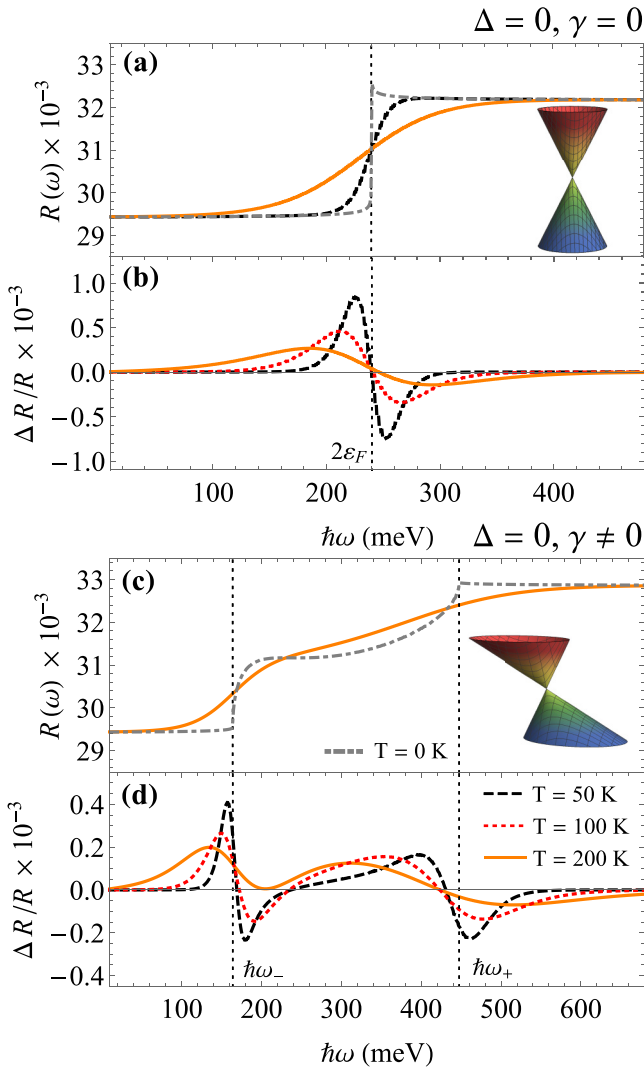
FIG. 2. Optical reflectivity $R(\omega)$ and its thermal derivative $\Delta R/R$ for several temperatures of the sample at normal incidence, corresponding to (a),(b) graphene and (c),(d) a gapless tilted anisotropic system (borophene 8-*Pmmn*). The insets illustrate the energy bands in each case. We use $\varepsilon_F = 120$ meV and $\Delta T = 1$ K.
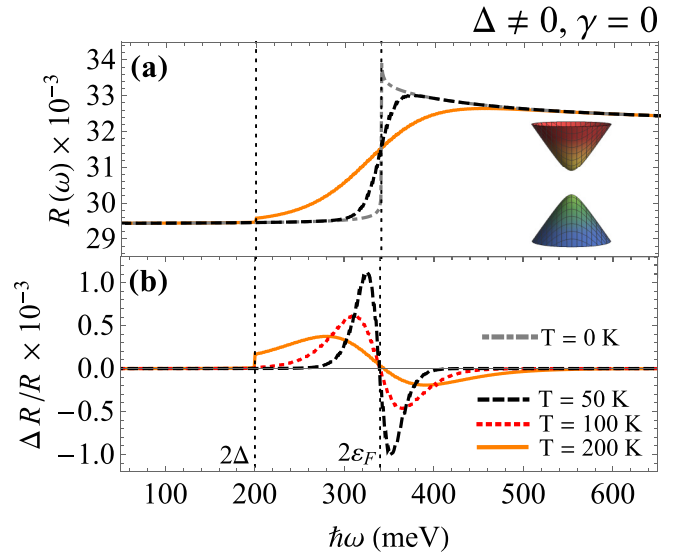

FIG. 3. (a) Optical reflectivity $R(\omega)$ and (b) its thermal derivative $\Delta R/R$ for several temperatures of the sample, corresponding to gapped graphene, with $\varepsilon_F > \Delta$. We take $\varepsilon_F = 170$ meV, $\Delta = 100$ meV, and $\Delta T = 1$ K.

the optical threshold at twice the Fermi energy splits into a couple of critical frequencies, $\hbar\omega_\pm = 2|\varepsilon_F|/(1 \mp \gamma)$ [21,22], as shown in the spectrum of reflectivity at zero temperature in Fig. 2(c). The sharp definition of such features is rapidly lost with increasing temperature. Notwithstanding, the thermal difference emphasizes $\hbar\omega_\pm$, as expected [Fig. 2(d)].

The case of a gapped material with cones without tilting is illustrated in Fig. 3 for gapped graphene. The spectra look similar to those of the gapless graphene [Figs. 2(a) and 2(b)], but now a feature appears at the energy gap 2Δ due to the onset for interband transitions. If ε_F lies within the gap, then this onset is the only salient feature in the spectra.

Figure 4 shows the results for a massive tilted system ($\gamma\Delta \neq 0$), corresponding to the cases $\varepsilon_F > \Delta$ [Figs. 4(a) and 4(b)] and $\tilde{\Delta} < \varepsilon_F < \Delta$ [Figs. 4(c) and 4(d)]. In the former case, the joint density of states (JDOS) at zero temperature displays two van Hove singularities at the energies [22]

$$\hbar\omega_\pm = \frac{2}{1-\gamma^2}\left(|\varepsilon_F| \pm \gamma\sqrt{\varepsilon_F^2 - \tilde{\Delta}^2}\right), \qquad (15)$$

and the optical conductivity tensor looks qualitatively similar to that of the case $\Delta = 0$, $\gamma \neq 0$ [Fig. 2(c)] [21,22]. As in the case of gapped graphene (Fig. 3), the reflectivity spectrum and its thermal difference show an optical feature at 2Δ due to the onset of interband transitions. In contrast, in the latter case, the JDOS develops three critical points, i.e., at 2Δ, $\hbar\omega_-$, and $\hbar\omega_+$, and a reduced overall size in comparison to the cases $\varepsilon_F < \tilde{\Delta}$ and $\varepsilon_F > \Delta$. Moreover, the number of interband transitions is strongly diminished between $\hbar\omega_-$ and $\hbar\omega_+$ because the k space available for transitions is considerably reduced. This behavior and the appearance of three critical points constitute an optical signature of the indirect gap [22]. As can be seen in Fig. 4(c), the feature at $\hbar\omega_-$ is lost even at small temperatures, and the derivative spectra do not clearly resolve the critical frequencies [Fig. 4(d)]. Moreover, besides the expected

atures [56]. It is worth noting that the function Λ in Eq. (14) becomes independent of tilting when $\Delta = 0$. Thus, for a fixed Fermi energy, the transcendental equation for $\mu(T)$ is exactly the same for the gapless cases with $\gamma = 0$ or $\gamma \neq 0$, as Fig. 1(b) illustrates. If we instead calculate $\mu(T)$ from Eq. (13) by fixing n, it would show different behavior for each case.

In Fig. 2, the spectrum of reflectivity R and the corresponding thermal difference, $\Delta R/R$, are shown for gapless Dirac systems and several temperature values at fixed ΔT. Figure 2(a) shows the isotropic case of doped graphene with a single optical threshold at frequency $2\varepsilon_F$ in the reflectivity spectrum at zero temperature. As the temperature increases, the spectral signature of the van Hove singularity is smoothed due to thermal broadening. However, the modulated spectrum shows a sharp feature around $2\varepsilon_F$ [Fig. 2(b)] that is still discernible for high temperatures. When the Dirac cone is tilted,
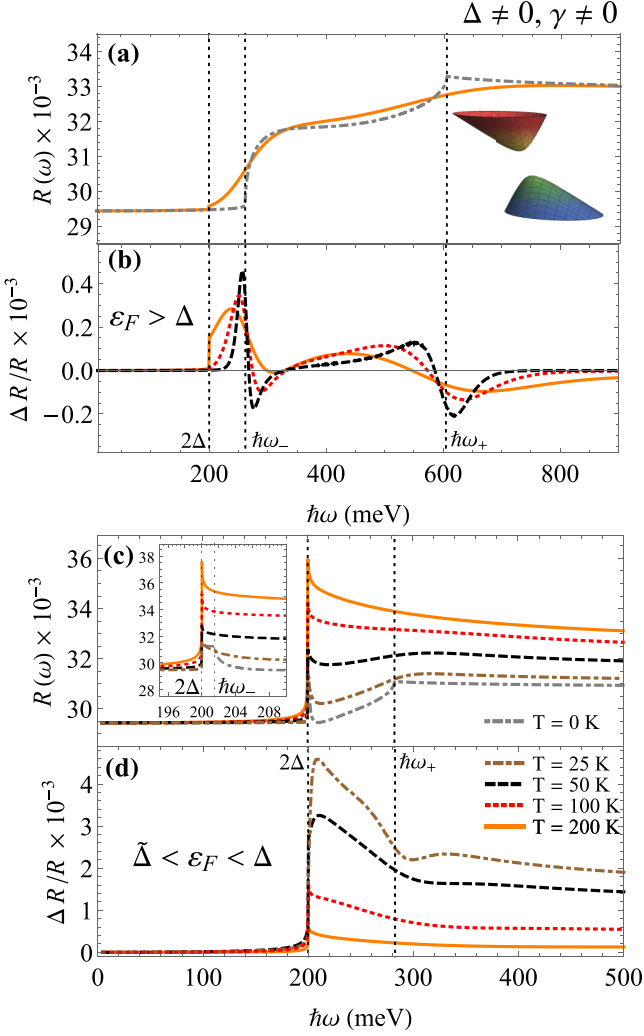
FIG. 4. Optical reflectivity and thermal derivative of a massive tilted Dirac system ($\Delta = 100$ meV) for several temperatures when the Fermi energy lies (a),(b) above the gap $\varepsilon_F > \Delta$ (with $\varepsilon_F = 170$ meV) and (c),(d) in the indirect zone $\tilde{\Delta} < \varepsilon_F < \Delta$ (with $\varepsilon_F = 95$ meV). The velocities v_i are taken as in borophene, and $\Delta T = 1$ K.

broadening, the reflectivity $R(\omega, T)$ increases slightly with temperature. This is because as the temperature increases, the peaked function $\partial f / \partial \mu' = \{4 k_B T \cosh^2 [\mu(T) - \mu']\}^{-1}$ is sampling the zero-temperature response $\sigma_{xx}(\omega, 0, \mu')$ in a μ' region where it appreciably increases because of the significant increase of the overall size of the JDOS when μ' moves out of the indirect zone, $\tilde{\Delta} < \mu' < \Delta$, in the integral (4) [22]. Such a gradient is a consequence of the simultaneous presence of tilting and gap, which introduces a new and narrow k-space region for allowed transitions, between the more extended regions corresponding to $\mu' < \tilde{\Delta}$ and $\mu' > \Delta$. Quantitatively, the integral (4) increases and causes a mild increase in reflectivity, as is shown in Fig. 4(c). This is in contrast to the situation observed in Fig. 4(a), where the convolution process involves a μ' region where the JDOS and the zero-temperature σ_{xx} do not present significant variation of its magnitude, leading just to a broadening. Note, however, that at finite temperature, the indirect nature of the gap is still traceable

from the spectra in the case $\varepsilon_F > \Delta$ [Figs. 4(a) and 4(b)] because the presence of the two features at $\hbar\omega_\pm$ suggests tilted cones, while the discontinuity at 2Δ reflects a gapped system.

For a doped system at finite temperature, the knowledge of the critical frequencies $\omega_\pm$ from the thermal difference spectrum suggests an efficient way to find the tilting parameter γ and the energy gap $\varepsilon_g = 2\tilde{\Delta}$. Using the definition of the kth power mean, $M_k = \{[(\hbar\omega_+)^k + (\hbar\omega_-)^k]/2\}^{1/k}$, we find, from Eq. (15),

$$\gamma^2 = 1 - 2|\varepsilon_F|/M_1, \tag{16}$$

$$\varepsilon_g = 2|\varepsilon_F| \left(\frac{M_{-1} - 2|\varepsilon_F|}{M_1 - 2|\varepsilon_F|} \right)^{1/2}, \tag{17}$$

where $M_1 = (\hbar\omega_+ + \hbar\omega_-)/2$ and $M_{-1} = 2(\hbar\omega_+)(\hbar\omega_-)/(\hbar\omega_+ + \hbar\omega_-)$ are the arithmetic and harmonic means of the numbers $\hbar\omega_\pm$, respectively.

We remark that Eqs. (16) and (17) are not restricted to the thermal differential technique that we propose; any optical method capable of critical frequencies determination could be useful to find the parameters γ and $\tilde{\Delta}$ through these equations. Here, we investigate an optical spectroscopy sensitive to temperature dependence and exemplify its use with massive tilted Dirac systems, although it could be applied in similar scenarios. This should be compared to the common use of differential techniques in 2D materials, oriented to mainly determine the degree of in-plane anisotropy.

In summary, we explore the joint density of states of doped massive tilted 2D Dirac systems through the temperature dependence of the reflectivity spectrum $R(\omega, T)$. The tilt of the bands increases the density of states and decreases the chemical potential function $\mu(T)$. On the other hand, the indirect gap of the energy dispersion notably modifies the optical conductivity spectrum as a function of the Fermi energy. Based on the difference of the reflectivity when the sample is held at two close temperatures, we obtain the fractional change $\Delta R/R$, which emphasizes the spectral structure associated to interband transitions, and probe its change due to variation of the Fermi level. The measurement of the critical energies in the optical response would allow one to estimate the magnitude of the tilting parameter and energy gap. Our results suggest that thermal difference spectroscopy is a plausible optical technique to identify such critical points despite the broadening of the spectra at finite temperature. The overall size of the derivative spectra shown here is of the same order of magnitude of the measured signals attained with current tools and they should be experimentally accessible. It was reported in [33] that Fermi-liquid corrections to the nonlocal optical conductivity could allow pure optical determination of the tilt. In light of our findings, the differential technique that we propose appears as an alternative. We hope that our work will stimulate further experiments and theory.

[1] *Photonic Probes of Surfaces*, Vol. 2, edited by P. Halevi (Elsevier Science B.V., North-Holland, Amsterdam, 1995).

[2] J. F. McGilp, Probing surface and interface structure using optics, J. Phys.: Condens. Matter **22**, 084018 (2010).

[3] L. Novotny and B. Hecht, *Principles of Nano-optics* (Cambridge University Press, Cambridge, 2012).

[4] M. Downer, Optics of surfaces and interfaces, Phys. Stat. Solidi (b) **253**, 197 (2016).

[5] X. Zhang, X. Han, F. Wu, J. Jasensky, and Z. Chen, Nano-bio interfaces probed by advanced optical spectroscopy: From model system studies to optical biosensors, Chinese Sci. Bull. **58**, 2537 (2013).

[6] G. Prévot, R. Bernard, H. Cruguel, A. Curcella, M. Lazzeri, T. Leoni, L. Masson, A. Ranguis, and Y. Borensztein, Formation of silicene on silver: Strong interaction between Ag and Si, Phys. Stat. Solidi (b) **253**, 206 (2016).

[7] A. K. Sarychev, A. Ivanov, A. N. Lagarkov, I. Ryzhikov, K. Afanasev, I. Bykov, G. Barbillon, N. Bakholdin, M. Mikhailov, A. Smyk, A. Shurygin, and A. Shalygin, Plasmon localization and giant fields in an open-resonator metasurface for surface-enhanced-raman-scattering sensors, Phys. Rev. Appl. **17**, 044029 (2022).

[8] S. Chang, X. Guo, and X. Ni, Optical metasurfaces: Progress and applications, Annu. Rev. Mater. Res. **48**, 279 (2018).

[9] S. Huang, C. Wang, Y. Xie, B. Yu, and H. Yan, Optical properties and polaritons of low symmetry 2D materials, Photon. Insight. **2**, R03 (2023).

[10] Q. Ma, G. Ren, K. Xu, and J. Z. Ou, Tunable optical properties of 2D materials and their applications, Adv. Opt. Mater. **9**, 2001313 (2021).

[11] X. Gan, D. Englund, D. Van Thourhout, and J. Zhao, 2D materials-enabled optical modulators: From visible to terahertz spectral range, Appl. Phys. Rev. **9**, 021302 (2022).

[12] W. Xin, H. B. Jiang, T. Q. Sun, X. G. Gao, S. N. Chen, B. Zhao, J. J. Yang, Z. B. Liu, J. G. Tian, and C. L. Guo, Optical anisotropy of black phosphorus by total internal reflection, Nano Mater. Sci. **1**, 304 (2019).

[13] C. Wang, G. Zhang, S. Huang, Y. Xie, and H. Yan, The optical properties and plasmonics of anisotropic 2D materials, Adv. Opt. Mater. **8**, 1900996 (2020).

[14] Q. Zhang, R. Zhang, J. Chen, W. Shen, C. An, X. Hu, M. Dong, J. Liu, and L. Zhu, Remarkable electronic and optical anisotropy of layered $1T'$-WTe$_2$ 2D materials, Beilstein J. Nanotechnol. **10**, 1745 (2019).

[15] W. Shen, C. Hu, J. Tao, J. Liu, S. Fan, Y. Wei, C. An, J. Chen, S. Wu, Y. Li, J. Liu, D. Zhang, L. Sun, and X. Hu, Resolving the optical anisotropy of low-symmetry 2D materials, Nanoscale **10**, 8329 (2018).

[16] L. Li, W. Han, L. Pi, P. Niu, J. Han, C. Wang, B. Su, H. Li, J. Xiong, Y. Bando, and T. Zhai, Emerging in-plane anisotropic two-dimensional materials, InfoMat **1**, 54 (2019).

[17] R. Frisenda, Y. Niu, P. Gant, A. J. Molina-Mendoza, R. Schmidt, R. Bratschitsch, J. Liu, L. Fu, D. Dumcenco, A. Kis, D. P. D. Lara, and A. Castellanos-Gomez, Micro-reflectance and transmittance spectroscopy: A versatile and powerful tool to characterize 2D materials, J. Phys. D **50**, 074002 (2017).

[18] Z. Zhou, Y. Cui, P.-H. Tan, X. Liu, and Z. Wei, Optical and electrical properties of two-dimensional anisotropic materials, J. Semiconduct. **40**, 061001 (2019).

[19] B. Sun, X. Gu, Q. Zeng, X. Huang, Y. Yan, Z. Liu, R. Yang, and Y. K. Koh, Temperature dependence of anisotropic thermal-conductivity tensor of bulk black phosphorus, Adv. Mater. **29**, 1603297 (2017).

[20] J. Tao, W. Shen, S. Wu, L. Liu, Z. Feng, C. Wang, C. Hu, P. Yao, H. Zhang, W. Pang, X. Duan, J. Liu, C. Zhou, and D. Zhang, Mechanical and electrical anisotropy of few-layer black phosphorus, ACS Nano **9**, 11362 (2015).

[21] S. Verma, A. Mawrie, and T. K. Ghosh, Effect of electron-hole asymmetry on optical conductivity in $8 - Pmmn$ borophene, Phys. Rev. B **96**, 155418 (2017).

[22] M. A. Mojarro, R. Carrillo-Bastos, and J. A. Maytorena, Optical properties of massive anisotropic tilted Dirac systems, Phys. Rev. B **103**, 165415 (2021).

[23] M. A. Mojarro, R. Carrillo-Bastos, and J. A. Maytorena, Hyperbolic plasmons in massive tilted two-dimensional Dirac materials, Phys. Rev. B **105**, L201408 (2022).

[24] C.-Y. Tan, J.-T. Hou, C.-X. Yan, H. Guo, and H.-R. Chang, Signatures of Lifshitz transition in the optical conductivity of two-dimensional tilted Dirac materials, Phys. Rev. B **106**, 165404 (2022).

[25] A. Wild, E. Mariani, and M. E. Portnoi, Optical absorption in two-dimensional materials with tilted Dirac cones, Phys. Rev. B **105**, 205306 (2022).

[26] C.-Y. Tan, C.-X. Yan, Y.-H. Zhao, H. Guo, and H.-R. Chang, Anisotropic longitudinal optical conductivities of tilted Dirac bands in $1T'-$MoS$_2$, Phys. Rev. B **103**, 125425 (2021).

[27] A. Balassis, G. Gumbs, and O. Roslyak, Polarizability, plasmons, and screening in 1T'-MoS$_2$ with tilted Dirac bands, Phys. Lett. A **449**, 128353 (2022).

[28] B. Fu, R.-W. Zhang, X. Fan, S. Li, D.-S. Ma, and C.-C. Liu, 2D ladder polyborane: An ideal Dirac semimetal with a multi-field-tunable band gap, ACS Nano **17**, 1638 (2023).

[29] S. H. Park, M. Sammon, E. Mele, and T. Low, Plasmonic gain in current biased tilted Dirac nodes, Nat. Commun. **13**, 7667 (2022).

[30] Z. Jalali-Mola and S. A. Jafari, Polarization tensor for tilted Dirac fermion materials: Covariance in deformed Minkowski spacetime, Phys. Rev. B **100**, 075113 (2019).

[31] T. Farajollahpour and S. A. Jafari, Synthetic non-Abelian gauge fields and gravitomagnetic effects in tilted Dirac cone systems, Phys. Rev. Res. **2**, 023410 (2020).

[32] Z. Jalali-Mola and S. A. Jafari, Undamped transverse electric mode in undoped two-dimensional tilted Dirac cone materials, Phys. Rev. B **102**, 245148 (2020).

[33] Z. Jalali-Mola and S. A. Jafari, Tilt-induced many-body corrections to optical conductivity of tilted Dirac cone materials, Phys. Rev. B **104**, 085152 (2021).

[34] E. Uykur, W. Li, C. A. Kuntscher, and M. Dressel, Optical signatures of energy gap in correlated Dirac fermions, npj Quantum Mater. **4**, 19 (2019).

[35] M. Hirata, K. Ishikawa, K. Miyagawa, M. Tamura, C. Berthier, D. Basko, A. Kobayashi, G. Matsuno, and K. Kanoda, Observation of an anisotropic Dirac cone reshaping and ferrimagnetic spin polarization in an organic conductor, Nat. Commun. **7**, 12666 (2016).

[36] M. Hirata, K. Ishikawa, G. Matsuno, A. Kobayashi, K. Miyagawa, M. Tamura, C. Berthier, and K. Kanoda, Anomalous spin correlations and excitonic instability of interacting 2D Weyl fermions, Science **358**, 1403 (2017).

[37] D. Ohki, M. Hirata, T. Tani, K. Kanoda, and A. Kobayashi, Chiral excitonic instability of two-dimensional tilted Dirac cones, Phys. Rev. Res. **2**, 033479 (2020).

[38] D. Ohki, K. Yoshimi, A. Kobayashi, and T. Misawa, Gap opening mechanism for correlated dirac electrons in organic compounds $\alpha-(\text{BEDT}-\text{TTF})_2\text{I}_3$ and $\alpha-(\text{BEDT}-\text{TSeF})_2\text{I}_3$, Phys. Rev. B **107**, L041108 (2023).

[39] A. Kobayashi, S. Katayama, Y. Suzumura, and H. Fukuyama, Massless fermions in organic conductor, J. Phys. Soc. Jpn. **76**, 034711 (2007).

[40] T. Osada and A. Kiswandhi, Possible current-induced phenomena and domain control in an organic Dirac fermion system with weak charge ordering, J. Phys. Soc. Jpn. **89**, 103701 (2020).

[41] K. Yoshimura, M. Sato, and T. Osada, Experimental confirmation of massive Dirac fermions in weak charge-ordering state in α-(BEDT-TTF)$_2$I$_3$, J. Phys. Soc. Jpn. **90**, 033701 (2021).

[42] Z.-Q. Wang, T.-Y. Lü, H.-Q. Wang, Y. P. Feng, and J.-C. Zheng, Band gap opening in 8-*Pmmn* borophene by hydrogenation, ACS Appl. Electron. Mater. **1**, 667 (2019).

[43] Y. Yekta, H. Hadipour, and S. A. Jafari, Tuning the tilt of the Dirac cone by atomic manipulations in 8*Pmmn* borophene, Commun. Phys. **6**, 46 (2023).

[44] M. J. Holcomb, J. P. Collman, and W. A. Little, Thermal difference spectroscopy, Rev. Sci. Instrum. **64**, 1862 (1993).

[45] M. J. Holcomb, J. P. Collman, and W. A. Little, Optical evidence of an electronic contribution to the pairing interaction in superconducting Tl$_2$Ba$_2$Ca$_2$Cu$_3$O$_{10}$, Phys. Rev. Lett. **73**, 2360 (1994).

[46] M. J. Holcomb, C. L. Perry, J. P. Collman, and W. A. Little, Thermal-difference reflectance spectroscopy of the high-temperature cuprate superconductors, Phys. Rev. B **53**, 6734 (1996).

[47] P. F. Maldague, Many-body corrections to the polarizability of the two-dimensional electron gas, Surf. Sci. **73**, 296 (1978).

[48] S. Nandy and D. A. Pesin, Low-energy effective theory and anomalous Hall effect in monolayer WTe$_2$, SciPost Phys. **12**, 120 (2022).

[49] H. Rostami and V. Juričić, Probing quantum criticality using nonlinear Hall effect in a metallic Dirac system, Phys. Rev. Res. **2**, 013069 (2020).

[50] Z. Z. Du, C. M. Wang, S. Li, H.-Z. Lu, and X. C. Xie, Disorder-induced nonlinear Hall effect with time-reversal symmetry, Nat. Commun. **10**, 3047 (2019).

[51] Z. Z. Du, C. M. Wang, H.-Z. Lu, and X. C. Xie, Band signatures for strong nonlinear Hall effect in bilayer WTe$_2$, Phys. Rev. Lett. **121**, 266601 (2018).

[52] S. Lahiri, K. Das, D. Culcer, and A. Agarwal, Intrinsic nonlinear conductivity induced by the quantum metric dipole, arXiv:2207.02178.

[53] P. Bhalla, K. Das, D. Culcer, and A. Agarwal, Resonant second-harmonic generation as a probe of quantum geometry, Phys. Rev. Lett. **129**, 227401 (2022).

[54] D.-K. Zhou, Z.-F. Zhang, X.-Q. Yu, Z.-G. Zhu, and G. Su, Fundamental distinction between intrinsic and extrinsic nonlinear thermal Hall effects, Phys. Rev. B **105**, L201103 (2022).

[55] E. V. Gorbar, V. P. Gusynin, V. A. Miransky, and I. A. Shovkovy, Magnetic field driven metal-insulator phase transition in planar systems, Phys. Rev. B **66**, 045108 (2002).

[56] A. Iurov, G. Gumbs, D. Huang, and G. Balakrishnan, Thermal plasmons controlled by different thermal-convolution paths in tunable extrinsic Dirac structures, Phys. Rev. B **96**, 245403 (2017).

[57] V. Y. Tsaran, A. V. Kavokin, S. G. Sharapov, A. A. Varlamov, and V. P. Gusynin, Entropy spikes as a signature of Lifshitz transitions in the Dirac materials, Sci. Rep. **7**, 10271 (2017).

[58] *Tables of Integrals, Series, and Products*, 8th ed., edited by D. Zwillinger, V. Moll, I. Gradshteyn, and I. Ryzhik (Academic Press, Boston, 2014).